Published in final edited form as:
*Opt Express*. 2009 March 2; 17(5): 4046–4060.

# Three-dimensional ultrahigh resolution optical coherence tomography imaging of age-related macular degeneration◇

**Yueli Chen**[1,2], **Laurel N. Vuong**[2], **Jonathan Liu**[1], **Joseph Ho**[2], **Vivek J. Srinivasan**[1], **Iwona Gorczynska**[1,2], **Andre J. Witkin**[2], **Jay S. Duker**[2], **Joel Schuman**[3], and **James G. Fujimoto**[1]

[1]Department of Electrical Engineering and Computer Science and Research Laboratory of Electronics, Massachusetts Institute of Technology, Cambridge, Massachusetts 02139

[2]New England Eye Center, Tufts Medical Center, Boston, Massachusetts 02116

[3]UPMC Eye Center, Dept. of Ophthalmology, University of Pittsburgh School of Medicine, Pittsburgh, PA

## Abstract

Ultrahigh resolution optical coherence tomography (OCT) enhances the ability to visualize different intra retinal layers. In age-related macular degeneration (AMD), pathological changes in individual retinal layers, including photoreceptor inner and outer segments and retinal pigment epithelium, can be detected. OCT using spectral / Fourier domain detection enables high speed, volumetric imaging of the macula, which provides comprehensive three-dimensional tomographic and morphologic information. We present a case series of AMD patients, from mild drusen to more advanced geographic atrophy and exudative AMD. Patients were imaged with a research prototype, ultrahigh resolution spectral / Fourier domain OCT instrument with 3.5 μm axial image resolution operating at 25,000 axial scans per second. These cases provide representative volumetric datasets of well-documented AMD pathologies which could be used for the development of visualization and imaging processing methods and algorithms.

## 1. Introduction

Optical Coherence Tomography (OCT) [1] is an emerging medical diagnostic imaging method enabling high resolution, cross-sectional imaging in biological tissues [2]. Ultrahigh resolution OCT (UHR-OCT) using a broadband light source improves axial image resolution to a few microns [3,4]. In ophthalmology, UHR-OCT is well suited for resolving individual retinal layers, because the orientation of these layers is roughly normal to the incident light [5,6]. Recently, advances in spectral / Fourier domain detection have greatly improved the sensitivity and imaging speed of OCT [7-14], enabling three-dimensional volumetric imaging of retinal structure, enhancing opportunities for clinical diagnostics and vision research. To date, OCT has become a well accepted clinical imaging modality in ophthalmology, where it has numerous applications for diagnosis of retinal disease, tracking disease progression, and response to therapy [15,16].

Age-related macular degeneration (AMD) is the leading cause of blindness in the elderly population in developed countries [17-20]. AMD can be classified into two subgroups, non-

◇Datasets associated with this article are available at http://hdl.handle.net/10376/1259



Corresponding author: jgfuji@mit.edu.

**OCIS codes:** (110.4500) Optical coherence tomography; (120.3180) Interferometry; (170.3880) Medical and biological imaging;

exudative (dry) AMD and exudative (wet) AMD. Non-exudative AMD comprises ninety percent of all diagnosed patients. It can progress to late stages, such as geographic atrophy and exudative (wet) AMD. In exudative AMD, severe visual loss is usually the result of leakage from choroidal neovascularization (CNV) [17,21-23]. Until recently, wet AMD accounted for about 88% of blindness in AMD. Diagnosis and treatment will become increasingly important as the average lifespan increases. Fluorescein angiography (FA) is the typical method to determine leakage from new vessels and indirectly detect CNV. AMD treatments include photodynamic therapy and anti-VEGF drugs such as ranibizumab and bevacizumab [24,25]. In addition, it is becoming increasingly important to monitor the progression of dry AMD, to assess changes in drusen and the retinal pigment epithelium (RPE) morphology [26,27]. Small amounts of hard drusen may not necessarily be a precursor to wet AMD, but confluent drusen are known to be associated with retinal pigment epithelium detachment (PED) and wet AMD. RPE changes such as atrophy result in photoreceptor degeneration and decreased visual acuity (VA).

Macular pathologies can be visualized with a number of methods including fundoscopic examination, color fundus photography, indocyanine green angiography, fundus autofluorescence, and FA. These techniques are basically *en face* imaging approaches. OCT, in contrast, is able to image cross-sections of retina. OCT has been shown to be very useful for macular disease detection [15,28]. Many pathological changes, such as subretinal fluid and RPE detachment, can be more easily identified from the cross-sectional view than *en face* view. Early studies demonstrated OCT for the diagnosis and monitoring of AMD [29] and other retinal diseases including macular holes, [30] glaucoma, [31] macular edema, [32] and diabetic retinopathy [33]. OCT was commercially developed in ophthalmology over a decade ago. The Stratus OCT from Carl Zeiss Meditec is currently considered the commercial standard for clinical OCT retinal imaging. The Stratus OCT uses time-domain detection and has ~10 μm axial resolution and an imaging speed of 400 axial scans per second. The speed allows acquisition of multiple 2-D OCT images, but limits the ability to perform three-dimensional imaging.

Ultrahigh resolution OCT (UHR-OCT), with ~3 μm axial image resolution was developed several years ago and demonstrated to enhance the visualization of individual retinal layers and intra-retinal pathology in macular diseases [3-6,34-37] UHR-OCT was especially interesting because it enabled visualization of the photoreceptor outer segments separately from the RPE. The junction between the photoreceptor inner and outer segments (IS/OS) boundary is highly reflective and provided a marker to visualize alterations in the photoreceptors and outer segments and photoreceptor impairment [34-42]. However, early UHR-OCT studies utilized time domain detection and imaging speeds were limited so that only individual cross-sectional images could be acquired.

High speed spectral / Fourier domain detection was a powerful advance because it significantly increased sensitivities and imaging speed [7-14]. The high speeds enabled raster scanning, which improved retinal coverage, avoiding sampling errors in the detection of focal pathologies, as well as three-dimensional, volumetric imaging. Three-dimensional datasets provide comprehensive information about retinal structure and can be used to extract retinal layer thickness maps, retinal nerve fiber layer thickness maps, as well as optic nerve head contour information [43]. To date, seven companies have developed spectral / Fourier domain OCT instruments for commercial use, which have been introduced to the ophthalmic market between 2006 and 2007. These instruments achieve 5 to 7 μm axial image resolutions and imaging speeds of 25,000 to 50,000 axial scans per second. Extensive studies using these commercial instruments are currently being performed and published. Laboratory instruments can achieve ultrahigh ~3 μm axial image resolutions and are now becoming commercially available. Even higher imaging speeds of >200,000 axial scans per second can be achieved

using swept source / Fourier domain OCT [44] or spectral / Fourier domain OCT using new high speed, line scan cameras [45].

Early studies using prototype high speed, ultrahigh resolution spectral / Fourier domain OCT instruments with ~3 μm axial image resolution demonstrated the ability to visualize details of retinal structure and pathology [16,43,46,47]. UHR spectral / Fourier domain OCT enables better visualization of outer retinal structure, but also increases the complexity of data interpretation and processing, since very fine retinal features can be visualized. The large amount of data which is generated makes manual examination of individual images impractical and highlights the need for improved automatic image analysis and visualization. In particular, the ability to quantitatively measure three-dimensional datasets in order to obtain parameters for early disease diagnosis or assessment of disease progression and response to treatment is becoming important.

Studies in the normal retina showed that structures in the outer retina and RPE could be quantitatively measured layer by layer using segmentation software [48]. Other studies applied semi-automated segmentation software to assess the outer retina near the RPE and photoreceptor outer segment region in patients with dry AMD [49]. A number of *en face* visualization methods have been developed to enable rapid assessment of pathology in three-dimensional OCT datasets [43,47,50,51] and a recent study of drusen in dry AMD was reported [52].

In this paper, we present a case series of three-dimensional UHR spectral / Fourier domain OCT datasets of patients with AMD, ranging from different types of drusen, to geographic atrophy and wet AMD. We encourage the use of these data by other parties who are interested in image processing and algorithm development. These datasets are obtained with higher axial resolution than most current, commercially available instruments, and therefore provide an opportunity to understand the challenges associated with processing of ultrahigh resolution datasets. Improvements in image resolution enable visualization of detailed structures, but also increase the size and complexity of the datasets, posing challenges for automated analysis and software development.

## 2. Materials and Methods

A research prototype UHR spectral / Fourier domain OCT system has been deployed in the New England Eye Center of the Tufts Medical Center since 2004. The system uses a broadband light source with three multiplexed superluminescent diodes (Broadlighter, Superlum) with a ~95 nm bandwidth at ~840 nm wavelength, which yields ~3.5 μm axial image resolution in the retina. The transverse image resolution is ~15−20 μm. The imaging speed is 25,000 axial scans per second. 3-D volumetric datasets comprised of 501 axial scans (of 1024 pixels each) per frame and a total of 180 frames acquired in ~4 seconds. The image volume is 6mm × 6mm × 1.3mm along the X (fast horizontal scan axis), Y (slow vertical scan axis) and Z (axial axis) directions, respectively. The incident power is 750 μW, comparable to exposure levels used in commercial instruments and within safe exposure limits determined by American National Standards Institute (ANSI).

Approximately 2000 patients have been enrolled for ultrahigh resolution OCT imaging at the New England Eye Center since 2004. The study protocol was approved by the institutional review boards of Tufts Medical Center, University of Pittsburgh Medical Center, and Massachusetts Institute of Technology. Written informed consent was obtained and the study conducted in accordance with Health Insurance Portability and Accountability Act (HIPAA). The datasets organized in this paper are a subset of typical AMD cases from more than 400 retinal scans using the prototype OCT system. The cases are arranged in a low-to-high severity

order based primarily on OCT image features. The RPE atrophy cases were selected from the dry AMD category. Wet AMD patients who appeared to have atrophy after treatment were excluded. One exudative AMD case with intraretinal fluid before and after ranibizumab treatment was included. For non-exudative AMD, automated segmentation of morphology in the photoreceptor outer segment and RPE region is currently a challenging issue. For exudative AMD, pathological changes, such as fluid volume, PED thickness mapping, and total macular volume are clinically interesting parameters. Representative datasets of these pathologies are therefore included.

Each 3D OCT dataset is stored in 180 two dimensional JPEG image files with a 256 level log gray scale. For each frame, the maximum signal and noise floor of log compressed data was calculated and this range was mapped to 256 linear gray scales. These image files are individual OCT frames along the fast scan axis. The data can be loaded into imaging processing software such as Matlab, OSA ISP, Amira, or other 3D processing packages. 3D-OCT data was obtained using a raster scan covering a 6mm × 6mm region of the macula. 180 cross-sectional, horizontal images (B-scans) separated by ~33 μm were acquired. Each B-scan had 501 transverse pixels (A-scans) separated by ~12 μm and each A-scan had 1024 points separated by 1.26 μm. The sequential B-scans have been corrected for axial eye motion by cross-correlating to detect motion and then translating the B-scan data in the axial direction. This enables the data to be viewed with reduced motion artifacts, but does not preserve the retinal contour in the vertical direction. Finally, it is important to note that the spatial aspect ratio of the 3-D images is different from the pixel aspect ratio. We preserved the original pixel aspect ratio without additional interpolation and therefore the image frames appears stretched along Z direction. To calculate the retinal volumes or other quantitative features, users should convert between spatial size 6mm × 6mm × 1.3mm and pixel dimension 501 × 180 × 1024.

## 3. Results

### 3.1 Drusen in Dry AMD

Drusen are localized deposits between the RPE and Bruch's membrane which are associated with AMD. In particular, large soft drusen have been considered as an important risk factor for advanced AMD. Drusen has various forms and classifications. In OCT, different types of drusen show different morphological structures and light scattering properties. Using ultrahigh resolution OCT, detailed architectural morphology, such as photoreceptor inner segment and outer segment junction (IS/OS), RPE, and Bruch's membrane can be visualized.

Figure 1 shows UHR spectral / Fourier domain OCT image data of the right eye of a 54 year old man with small hard drusen and a visual acuity of 20/20. The *en face* OCT fundus image (top-left) is the projection or axial summation of the 3D retinal image volume along the Z direction. This *en face* OCT image shows scattering intensity variation in the foveal region, corresponding to the yellowish, highly scattering spots in the color fundus photo (bottom-left). The rectangle shown corresponds to the size of OCT *en face* view. 3D-OCT imaging precisely registers the *en face* view to the OCT cross-sectional frames since the *en face* view is constructed directly from the volumetric dataset. The right side of Fig. 1 shows three selected OCT cross-sectional near the fovea, at the positions shown in the *en face* image. Small, discrete drusen (white arrows) can be seen which have altered the normal contour of the photoreceptor outer segments and RPE. The retinal layers are resolved with UHR spectral / Fourier domain OCT and are labeled in the middle OCT image.

Figure 2 shows image data from the right eye of a 58 year old female with dry AMD and a visual acuity of 20/25. In this case, the accumulated drusen not only altered the morphology of RPE, but also appear to have caused photoreceptor disruption, as evidenced by the loss of the inner and outer segment (IS/OS) junction at several locations (thin arrows). The normal IS/

OS junction should appear as a strong, well defined scattering line in OCT images. Thinning of the outer nuclear layer is also visible above the areas of drusen elevation. Bruch's membrane can be seen beneath the large drusen (solid arrow). In the normal eye, Bruch's membrane is not visible because it is directly adjacent to the RPE.

Figure 3 shows image data from the left eye of a 60 year old female with dry AMD diagnosed in both eyes. The visual acuity in her left eye was 20/40. From the three selected cross-sectional OCT images, it is clearly observable that small lesions of soft drusen “merge” to form confluent drusen (solid arrows). The complicated morphology in the RPE is the result of coalescence of drusen of various sizes at different locations. The confluent drusen deposits appear as moderately strong scattering areas below the RPE. This case shows typical confluent drusen in AMD, where the photoreceptor IS/OS junction follows the morphological elevation of the RPE. The curvature of the boundary is generally smooth, without sudden discontinuities. However, at some locations, the drusen deposits seem to penetrate into the photoreceptors, disrupting the photoreceptor IS/OS boundary (thin arrow). From the *en face* OCT fundus view (top-left) the confluent drusen appear as moderately scattering areas, with smooth, low scattering boundaries (see arrow head).

Figure 4 shows UHR spectral / Fourier domain OCT data from the left eye of a 91 year old female diagnosed with AMD. The patient's visual acuity was limited to counting fingers at 5 feet (CF 5’). The selected cross-sectional OCT images show a lesion with a diameter of about 1.5 mm. The normal foveal contour is disrupted and there is significant elevation of the RPE, consistent with retinal pigment epithelial detachment (PED). Photoreceptor impairment is visible as loss of the IS/OS boundary in some areas (thin arrow) above the drusen, suggesting the role of drusen in disease progression and vision impairment. Atrophy of the photoreceptors, with pronounced thinning of the photoreceptor outer nuclear layer can also be seen. Bruch's membrane can be seen as a thin, scattering line, adjacent to the choriocapillaris, where the normal RPE should be (small solid arrow, bottom image). RPE elevation and photoreceptor disruption is present over a much larger region of the fundus, with greater irregularities observed in the cross-sectional OCT images, compared with the previous case (Fig. 3).

### 3.2 RPE Atrophy

Figure 5 shows UHR spectral / Fourier domain OCT data from the right eye of a 67 year old male with dry AMD and a visual acuity of 20/40. The fundus image shows that the fovea has a significant amount of drusen deposits, but no fluid was detected. The OCT cross-sectional images superior to the macula revealed irregular and discontinuous photoreceptor and RPE layers (arrow head). The hyper-scattering signal observed below the RPE in the choroid is the result of the RPE degeneration. When the RPE layer is normal, the melanin pigment will attenuate the OCT beam and reduce the back scattering intensity from the choroid. Above the hyper reflective area, the normal IS/OS junction and RPE layers are not present. Bruch's membrane and choriocapillaris become visible (small white arrows). In the OCT image of a normal eye, Bruch's membrane could not be discerned from RPE. Although OCT imaging shows RPE degeneration indirectly as a change in optical properties, the ability to assess light penetration makes OCT a very sensitive method for detecting RPE atrophy.

Figure 6 shows a typical case of geographic atrophy with image data from the left eye of an 84 year old female with a visual acuity of 20/160. Geographic atrophy is the advanced stage of dry AMD which impairs vision through the loss of photoreceptors. Geography atrophy appears as white, highly scattering regions on the *en face* OCT image and loss of pigmentation on the fundus photo (arrow head). Cross-sectional OCT images show that the hyper-scattering originates from loss of the RPE and increased light penetration into the choroid (white arrows). The normal photoreceptor IS/OS junction and RPE are absent in the area of atrophy. In contrast, Bruch's membrane, which is normally not visible because of the adjacent RPE and

choriocapilaris, is seen in the position corresponding to where the normal RPE should be. Note that in our scan protocol, the zero delay was placed at choroid / sclera to enhance the signal of deeper structure. Because OCT scans of geographic atrophy patients show deeper penetration and usually more axial motion due to difficulty in eye fixation, mirroring effect at zero delay was observed in some frames for this case.

### 3.3 Exudative AMD and response to treatment

Exudative (wet) AMD is another advanced form of AMD. Compared to the dry form of AMD, exudative AMD is characterized by formation of abnormal choroidal neovascular lesions which leak fluid and blood into the macula, ultimately causing destruction of the photoreceptors and RPE. To date, fluorescein angiography is the most sensitive and widely used method to diagnose wet AMD. Anti-VEGF drugs, including ranibizumab and bevacizumab were recently found to effectively reduce the neovascularization and fluid volume [24,25]. The following section presents a representative example of OCT imaging of a subject with wet AMD before and after treatment by ranibizumab injection.

A 77 year old female was diagnosed with exudative AMD in her right eye before ranibizumab treatment (Fig. 7). Fluorescein angiography at 67 seconds (Fig. 7B) and 5 minutes (Fig. 7C) indicate the presence of choroidal neovascularization. OCT cross-sectional images reveal the presence of intraretinal and subretinal fluid (small arrows). Similar to the case in Fig. 4, the detached Bruch's membrane (thin arrow) indicates PED. In this case, the PED is caused by a choroidal neovascular membrane growing between the RPE and Bruch's membrane. This fibrovascular PED is composed of abnormal blood vessels, fibrous tissue, and fluid, and therefore appear more highly back-scattering on OCT than fluid alone. The thickened RPE likely arises from disruption of the RPE overlying the CNV, as well as abnormal blood vessels growing between the RPE and the retina. The patient was treated that day with an intraocular ranibizumab injection, and returned one month after treatment for repeat imaging using UHR spectral / Fourier domain OCT. The fluid volume was significantly reduced (Fig. 8). The subject's visual acuity was counting fingers at 4 feet (CF4') before treatment and counting fingers at 5 feet (CF5') after treatment. OCT imaging revealed a decrease in subretinal fluid, but the fibrovascular PED was largely unchanged. These results show that OCT can be used to detect wet AMD and monitor progression of the disease, by longitudinally comparing changes in retinal pathology.

## 4. Discussion

This manuscript presents a cross-section of AMD cases imaged with UHR spectral / Fourier domain OCT at 3.5 μm axial image resolution. Cases were selected from over 800 AMD patients and include small hard drusen, larger confluent drusen, PED, geographic atrophy and wet AMD with choroidal neovascularization. The changes in retinal architectural morphology between different stages of AMD can be appreciated in great detail using volumetric UHR spectral / Fourier domain OCT imaging. However, in spite of the improved visualization and retinal coverage provided by ultrahigh resolution volumetric datasets, 3D-OCT imaging poses significant challenges. Datasets are large and therefore it is impractical and time consuming to review data on an image-by-image basis. Three-dimensional rendering methods can help to visualize three-dimensional structures, but seem to have limited effectiveness over conventional methods for diagnosis or assessing the progression of disease. In current clinical practice, the majority of ophthalmologists use printed summaries of OCT image data for diagnosis. Online viewing and manipulation of three-dimensional datasets is time consuming and considered impractical for widespread clinical use.

The development of automated / intelligent software which can identify and quantitatively measure focal pathologies is especially important. In wet AMD, the ability to measure the

volume and area of subretinal fluid, CNV and PED is important for assessing response to anti-VEGF therapies and the need for re-treatment. The assessment of wet AMD is challenging because of the complex nature of the pathology, loss of normal retinal architecture and changes in image contrast, which make automated identification and segmentation of lesions difficult. Image processing algorithms which work well in the normal retina, can have unacceptable error rates in the presence of pathology.

With the recent interest in new pharmacological approaches to treat dry AMD, quantitative assessment of early stage disease is becoming important. This task is also challenging due to the focal nature of the lesions. Drusen appear in large numbers and are associated with subtle alterations in the photoreceptor outer segments, RPE and Bruch's membrane. The ability to automatically measure the total area of volume of drusen would be an important advance, but is difficult because of the small size and multifocal nature of these lesions. Small errors in automatic segmentation might yield significant variations in measurement and repeatability of measurement promise to be an important issue. Quantitative assessment of photoreceptor integrity is also an intriguing concept. The ability to assess the integrity of the inner and outer segment boundary might be easier than assessment of drusen and could be a promising approach. It may also be possible to identify other more advanced image features which assess photoreceptor integrity, such as thickening of the RPE, changes in Bruch's membrane, or atrophy in the outer nuclear layer.

Ultimately, clinical studies will be required which can evaluate the validity of 3D-OCT image parameters as surrogate markers of disease or disease progression. In the context of AMD, one key issue is the correlation of structural change to loss of visual function. Correlation of simple visual acuity measurement and structural change will undoubtedly be challenging, because similar pathology in different regions of the macula would have a dramatically different impact on acuity. However, correlation of structure and function using techniques such as multifocal ERG or microperimetry may be promising, since they could enable registration of structural changes to functional responses across the fundus.

The development of advanced image processing techniques in combination with the recent advances in ultrahigh resolution and high speed OCT imaging promises to be a powerful advance which will enable the full potential of very large, three-dimensional volumetric datasets to be realized. The development of quantitative methods to assess pathology and their validation as surrogate markers for early diagnosis, disease progression, or response to therapy promises to yield important advances across multiple fields ranging from fundamental research in disease pathogenesis, drug development, and more effective clinical care.

## Acknowledgments

Dr. Iwona Gorczynska's present address is the Institute of Physics, Nicolaus Copernicus University, Toruń, Poland. Dr. Srinivasan's present address it the Martinos Imaging Center of the Massachusetts General Hospital, Boston, MA. The authors would like to acknowledge the research support from the National Institutes of Health R01-EY11289-23, R01-EY13178-07, P30-EY008098; National Science Foundation BES-0522845; Air Force Office of Scientific Research, FA9550-07-1-0014 and Medical Free Electron Laser Program contract FA9550-07-1-0101; Massachusetts Lions Eye Research Fund; and Research to Prevent Blindness Unrestricted Grant.

## References and links

1. Huang D, Swanson EA, Lin CP, Schuman JS, Stinson WG, Chang W, Hee MR, Flotte T, Gregory K, Puliafito CA, Fujimoto JG. Optical Coherence Tomography. Science 1991;254:1178–1181. [PubMed: 1957169]
2. Fujimoto JG. Optical coherence tomography for ultrahigh resolution in vivo imaging. Nature Biotechnology 2003;21:1361–1367.

3. Drexler W, Morgner U, Kartner FX, Pitris C, Boppart SA, Li XD, Ippen EP, Fujimoto JG. In vivo ultrahigh-resolution optical coherence tomography. Opt. Lett 1999;24:1221–1223. [PubMed: 18073990]
4. Drexler W, Morgner U, Ghanta RK, Kärtner FX, Schuman JS, Fujimoto JG. Ultrahigh-resolution ophthalmic optical coherence tomography. Nature Medicine 2001;7:502–507.
5. Gloesmann M, Hermann B, Schubert C, Sattmann H, Ahnelt PK, Drexler W. Histologic correlation of pig retina radial stratification with ultrahigh-resolution optical coherence tomography. Investigative Ophthalmology & Visual Science 2003;44:1696–703. [PubMed: 12657611]
6. Anger EM, Unterhuber A, Hermann B, Sattmann H, Schubert C, Morgan JE, Cowey A, Ahnelt PK, Drexler W. Ultrahigh resolution optical coherence tomography of the monkey fovea. Identification of retinal sublayers by correlation with semithin histology sections. Experimental Eye Research 2004;78:1117–25. [PubMed: 15109918]
7. Wojtkowski M, Leitgeb R, Kowalczyk A, Bajraszewski T, Fercher AF. In vivo human retinal imaging by Fourier domain optical coherence tomography. J Biomed Opt 2002;7:457–463. [PubMed: 12175297]
8. Choma MA, Sarunic MV, Yang CH, Izatt JA. Sensitivity advantage of swept source and Fourier domain optical coherence tomography. Opt. Express 2003;11:2183–2189. [PubMed: 19466106]
9. de Boer JF, Cense B, Park BH, Pierce MC, Tearney GJ, Bouma BE. Improved signal-to-noise ratio in spectral-domain compared with time-domain optical coherence tomography. Opt. Lett 2003;28:2067–2069. [PubMed: 14587817]
10. Leitgeb R, Hitzenberger CK, Fercher AF. Performance of Fourier domain vs. time domain optical coherence tomography. Opt. Express 2003;11:889–894. [PubMed: 19461802]
11. Wojtkowski M, Bajraszewski T, Targowski P, Kowalczyk A. Real-time in vivo imaging by high-speed spectral optical coherence tomography. Opt. Lett 2003;28:1745–1747. [PubMed: 14514087]
12. Nassif NA, Cense B, Park BH, Pierce MC, Yun SH, Bouma BE, Tearney GJ, Chen TC, de Boer JF. In vivo high-resolution video-rate spectral-domain optical coherence tomography of the human retina and optic nerve. Opt. Express 2004;12:367–376. [PubMed: 19474832]
13. Cense B, Nassif NA, Chen TC, Pierce MC, Yun SH, Park BH, Bouma BE, Tearney GJ, de Boer JF. Ultrahigh-resolution high-speed retinal imaging using spectral-domain optical coherence tomography. Opt. Express 2004;12:2435–2447. [PubMed: 19475080]
14. Wojtkowski M, Srinivasan VJ, Ko TH, Fujimoto JG, Kowalczyk A, Duker JS. Ultrahigh-resolution, high-speed, Fourier domain optical coherence tomography and methods for dispersion compensation. Optics Express 2004;12:2404–2422. [PubMed: 19475077]
15. Schuman, JS.; Puliafito, CA.; Fujimoto, JG. Optical coherence tomography of ocular diseases. 2nd edition. Slack Inc; Thorofare, NJ: 2004.
16. Drexler W, Fujimoto JG. State-of-the-art retinal optical coherence tomography. Prog Retin Eye Res 2008;27:45–88. [PubMed: 18036865]
17. Green WR, Key SN 3rd. Senile macular degeneration: a histopathologic study. Trans Am Ophthalmol Soc 1977;75:180–254. [PubMed: 613523]
18. Klein R, Klein BE, Jensen SC, Meuer SM. The five-year incidence and progression of age-related maculopathy: the Beaver Dam Eye Study. Ophthalmology 1997;104:7–21. [PubMed: 9022098]
19. Friedman DS, O'Colmain BJ, Munoz B, Tomany SC, McCarty C, de Jong PT, Nemesure B, Mitchell P, Kempen J. Prevalence of age-related macular degeneration in the United States. Arch Ophthalmol 2004;122:564–72. [PubMed: 15078675]
20. de Jong PT. Age-related macular degeneration. N. Engl. J. Med 2006;355:1474–85. [PubMed: 17021323]
21. Chamberlin JA, Bressler NM, Bressler SB, Elman MJ, Murphy RP, Flood TP, Hawkins BS, Maguire MG, Fine SL. The use of fundus photographs and fluorescein angiograms in the identification and treatment of choroidal neovascularization in the Macular Photocoagulation Study. The Macular Photocoagulation Study Group. Ophthalmology 1989;96:1526–34. [PubMed: 2479899]
22. M.P.S. Group. Persistent and recurrent neovascularization after laser photocoagulation for subfoveal choroidal neovascularization of age-related macular degeneration. Macular Photocoagulation Study Group. Arch Ophthalmol 1994;112:489–99. [PubMed: 7512335]

23. M.P.S. Group. Visual outcome after laser photocoagulation for subfoveal choroidal neovascularization secondary to age-related macular degeneration. The influence of initial lesion size and initial visual acuity. Macular Photocoagulation Study Group. Arch Ophthalmol 1994;112:480–8. [PubMed: 7512334]
24. Avery RL, Pieramici DJ, Rabena MD, Castellarin AA, Nasir MA, Giust MJ. Intravitreal bevacizumab (Avastin) for neovascular age-related macular degeneration. Ophthalmology 2006;113:363–372. [PubMed: 16458968]
25. Rosenfeld PJ, Rich RM, Lalwani GA. Ranibizumab: Phase III Clinical Trial Results. Ophthalmol Clin North Am 2006;19:361–72. [PubMed: 16935211]
26. Abdelsalam A, Del Priore L, Zarbin MA. Drusen in age-related macular degeneration: pathogenesis, natural course, and laser photocoagulation-induced regression. Surv Ophthalmol 1999;44:1–29. [PubMed: 10466585]
27. Zarbin MA. Current concepts in the pathogenesis of age-related macular degeneration. Arch Ophthalmol 2004;122:598–614. [PubMed: 15078679]
28. Puliafito CA, Hee MR, Lin CP, Reichel E, Schuman JS, Duker JS, Izatt JA, Swanson EA, Fujimoto JG. Imaging of macular diseases with optical coherence tomography. Ophthalmology 1995;102:217–229. [PubMed: 7862410]
29. Hee MR, Baumal CR, Puliafito CA, Duker JS, Reichel E, Wilkins JR, Coker JG, Schuman JS, Swanson EA, Fujimoto JG. Optical coherence tomography of age-related macular degeneration and choroidal neovascularization. Ophthalmology 1996;103:1260–1270. [PubMed: 8764797]
30. Hee MR, Puliafito CA, Wong C, Duker JS, Reichel E, Schuman JS, Swanson EA, Fujimoto JG. Optical coherence tomography of macular holes. Ophthalmology 1995;102:748–756. [PubMed: 7777274]
31. Schuman JS, Hee MR, Arya AV, Pedut-Kloizman T, Puliafito CA, Fujimoto JG, Swanson EA. Optical coherence tomography: a new tool for glaucoma diagnosis. Current Opinion in Ophthalmology 1995;6:89–95. [PubMed: 10150863]
32. Hee MR, Puliafito CA, Wong C, Duker JS, Reichel E, Rutledge B, Schuman JS, Swanson EA, Fujimoto JG. Quantitative assessment of macular edema with optical coherence tomography. Archives of Ophthalmology 1995;113:1019–1029. [PubMed: 7639652]
33. Hee MR, Puliafito CA, Duker JS, Reichel E, Coker JG, Wilkins JR, Schuman JS, Swanson EA, Fujimoto JG. Topography of diabetic macular edema with optical coherence tomography. Ophthalmology 1998;105:360–370. [PubMed: 9479300]
34. Drexler W, Sattmann H, Hermann B, Ko TH, Stur M, Unterhuber A, Scholda C, Findl O, Wirtitsch M, Fujimoto JG, Fercher AF. Enhanced visualization of macular pathology with the use of ultrahigh-resolution optical coherence tomography. Archives of Ophthalmology 2003;121:695–706. [PubMed: 12742848]
35. Ko TH, Fujimoto JG, Duker JS, Paunescu LA, Drexler W, Baumal CR, Puliafito CA, Reichel E, Rogers AH, Schuman JS. Comparison of ultrahigh- and standard-resolution optical coherence tomography for imaging macular hole pathology and repair. Ophthalmology 2004;111:2033–2043. [PubMed: 15522369]
36. Ko TH, Fujimoto JG, Schuman JS, Paunescu LA, Kowalevicz AM, Hartl I, Drexler W, Wollstein G, Ishikawa H, Duker JS. Comparison of ultrahigh- and standard-resolution optical coherence tomography for imaging macular pathology. Ophthalmology 2005;112:1922, e1–15. [PubMed: 16183127]
37. Ergun E, Hermann B, Wirtitsch M, Unterhuber A, Ko TH, Sattmann H, Scholda C, Fujimoto JG, Stur M, Drexler W. Assessment of central visual function in Stargardt's disease/fundus flavimaculatus with ultrahigh-resolution optical coherence tomography. Investigative Ophthalmology & Visual Science 2005;46:310–316. [PubMed: 15623790]
38. Wirtitsch MG, Ergun E, Hermann B, Unterhuber A, Stur M, Scholda C, Sattmann H, Ko TH, Fujimoto JG, Drexler W. Ultrahigh resolution optical coherence tomography in macular dystrophy. American Journal of Ophthalmology 2005;140:976–983. [PubMed: 16376639]
39. Ko TH, Witkin AJ, Fujimoto JG, Chan A, Rogers AH, Baumal CR, Schuman JS, Drexler W, Reichel E, Duker JS. Ultrahigh-resolution optical coherence tomography of surgically closed macular holes. Arch. Ophthalmol 2006;124:827–836. [PubMed: 16769836]

40. Paunescu LA, Ko TH, Duker JS, Chan A, Drexler W, Schuman JS, Fujimoto JG. Idiopathic juxtafoveal retinal telangiectasis: new findings by ultrahigh-resolution optical coherence tomography. Ophthalmology 2006;113:48–57. [PubMed: 16343625]
41. Scholda C, Wirtitsch M, Hermann B, Unterhuber A, Ergun E, Sattmann H, Ko TH, Fujimoto JG, Fercher AF, Stur M, Schmidt-Erfurth U, Drexler W. Ultrahigh resolution optical coherence tomography of macular holes. Retina 2006;26:1034–1041. [PubMed: 17151491]
42. Witkin AJ, Ko TH, Fujimoto JG, Chan A, Drexler W, Schuman JS, Reichel E, Duker JS. Ultra-high resolution optical coherence tomography assessment of photoreceptors in retinitis pigmentosa and related diseases. American Journal of Ophthalmology 2006;142:945–952. [PubMed: 17157580]
43. Wojtkowski M, Srinivasan V, Fujimoto JG, Ko T, Schuman JS, Kowalczyk A, Duker JS. Three-dimensional retinal imaging with high-speed ultrahigh-resolution optical coherence tomography. Ophthalmology 2005;112:1734–1746. [PubMed: 16140383]
44. Srinivasan VJ, Adler DC, Chen Y, Gorczynska I, Huber R, Duker JS, Schuman JS, Fujimoto JG. Ultrahigh-speed optical coherence tomography for three-dimensional and en face imaging of the retina and optic nerve head. Investigative Ophthalmology & Visual Science 2008;49:5103–5110. [PubMed: 18658089]
45. Potsaid B, Gorczynska I, Srinivasan VJ, Chen Y, Jiang J, Cable A, Fujimoto JG. Ultrahigh speed spectral / Fourier domain OCT ophthalmic imaging at 70,000 to 312,500 axial scans per second. Opt Express 2008;16:15149–15169. [PubMed: 18795054]
46. Schmidt-Erfurth U, Leitgeb RA, Michels S, Povazay B, Sacu S, Hermann B, Ahlers C, Sattmann H, Scholda C, Fercher AF, Drexler W. Three-dimensional ultrahigh-resolution optical coherence tomography of macular diseases. Investigative Ophthalmology & Visual Science 2005;46:3393–3402. [PubMed: 16123444]
47. Srinivasan VJ, Wojtkowski M, Witkin AJ, Duker JS, Ko TH, Carvalho M, Schuman JS, Kowalczyk A, Fujimoto JG. High-definition and 3-dimensional imaging of macular pathologies with high-speed ultrahigh-resolution optical coherence tomography. Ophthalmology 2006;113:2054–2065. [PubMed: 17074565]
48. Srinivasan VJ, Monson BK, Wojtkowski M, Bilonick RA, Gorczynska I, Chen R, Duker JS, Schuman JS, Fujimoto JG. Characterization of outer retinal morphology with high-speed, ultrahigh-resolution optical coherence tomography. Investigative Ophthalmology & Visual Science 2008;49:1571–1579. [PubMed: 18385077]
49. Szkulmowski M, Wojtkowski M, Sikorski B, Bajraszewski T, Srinivasan VJ, Szkulmowska A, Kaluzny JJ, Fujimoto JG, Kowalczyk A. Analysis of posterior retinal layers in spectral optical coherence tomography images of the normal retina and retinal pathologies. J. Biomed. Opt 2007;12
50. Jiao SL, Knighton R, Huang XR, Gregori G, Puliafito CA. Simultaneous acquisition of sectional and fundus ophthalmic images with spectral-domain optical coherence tomography. Opt. Express 2005;13:444–452. [PubMed: 19488371]
51. Jiao SL, Wu CY, Knighton RW, Gregori G, Puliafito CA. Registration of high-density cross sectional images to the fundus image in spectral-domain ophthalmic optical coherence tomography. Opt. Express 2006;14:3368–3376. [PubMed: 19516481]
52. Gorczynska I, Srinivasan VJ, Vuong LN, Chen RW, Liu JJ, Reichel E, Wojtkowski M, Schuman JS, Duker JS, Fujimoto JG. Projection OCT fundus imaging for visualizing outer retinal pathology in non-exudative age related macular degeneration. Br. J. Ophthalmol. 2008 epub doi:10.1136.

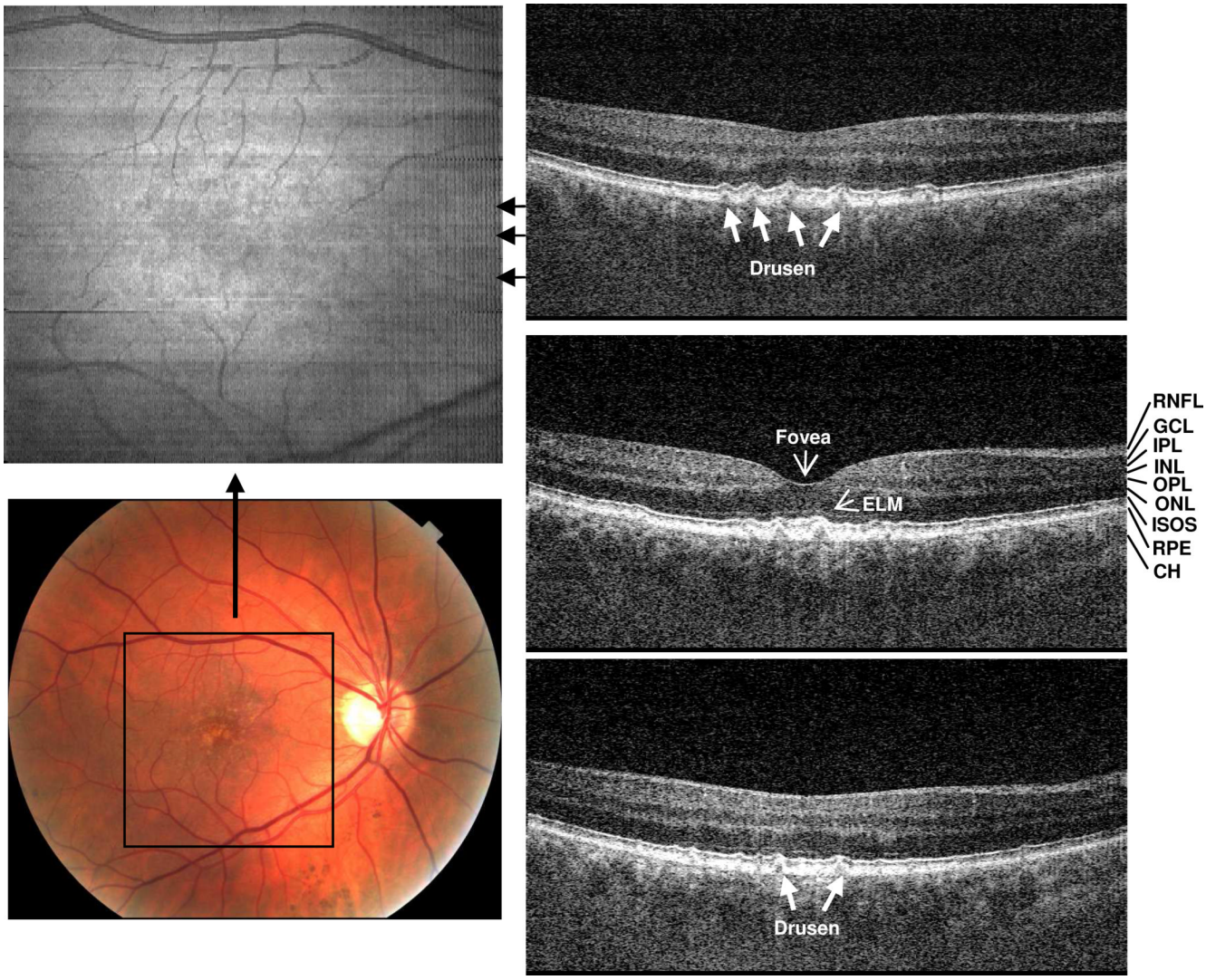


**Fig. 1.**

Ultrahigh resolution, spectral / Fourier domain OCT volumetric dataset and fundus photograph of the right eye of a 54 year old male subject with mild dry AMD (View 1). The en face OCT fundus image (top-left) is generated by axial summation of the 3D-OCT dataset. Color fundus photo (bottom-left) showing the location of the 3D-OCT volumetric data. Three OCT cross-sectional images are selected from superior to inferior near fovea to show representative pathology. The positions of the OCT images are marked with black arrows on the en face OCT fundus image. Discrete drusen can be seen in the fundus images and in corresponding positions in the OCT cross-sectional images. Ultrahigh resolution enables most of the individual retinal layers to be resolved. RNFL: retinal nerve fiber layer, GCL: ganglion cell layer, OPL: outer plexiform layer, ONL: outer nuclear layer, IPL: inner plexiform layer, INL: inner nuclear layer, ELM: external limiting membrane, IS/OS: photoreceptor inner and outer segment junction, RPE: retinal pigmented epithelium, and CH: choroid.

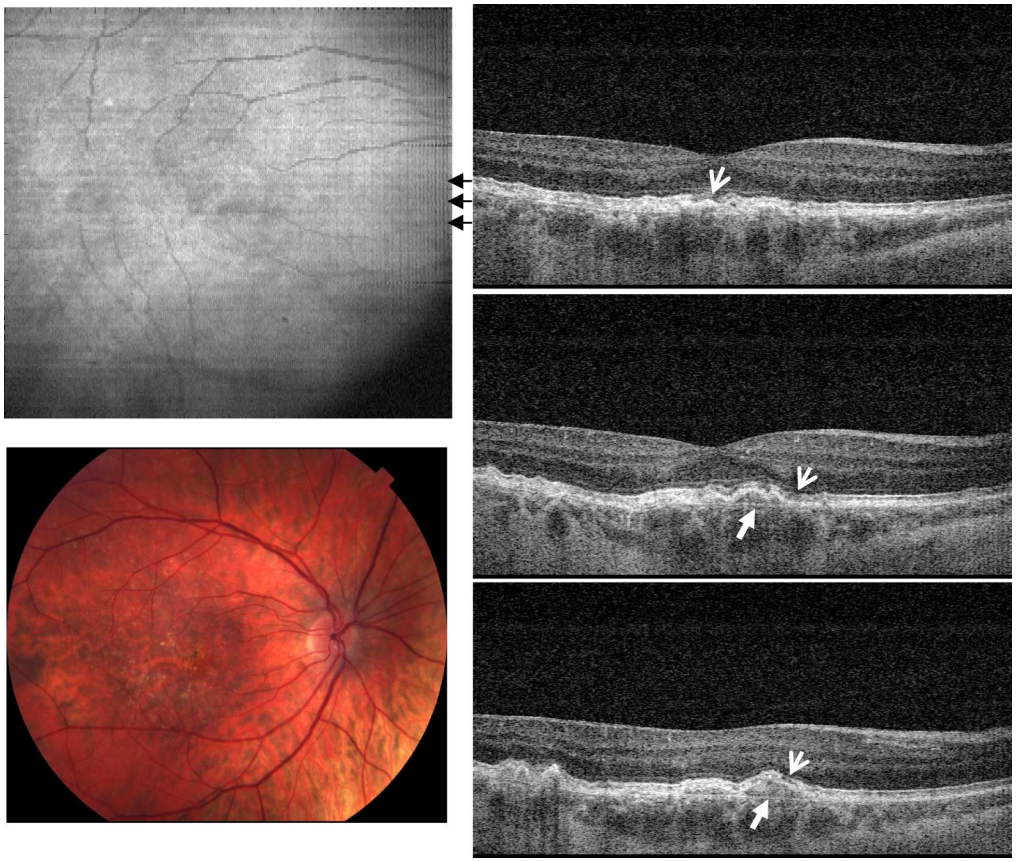

**Fig. 2.**

Image data from the right eye of a 58 year old female subject diagnosed with dry AMD in both eyes (View 2). Her right eye had a visual acuity of 20/25. The OCT cross-sectional images show elevation of the RPE due to drusen and changes in the photoreceptor inner and outer segment (IS/OS) boundary (thin arrows). Bruch's membrane appears under the area with large drusen deposits (solid arrows), but is not visible in the normal areas of the retina.

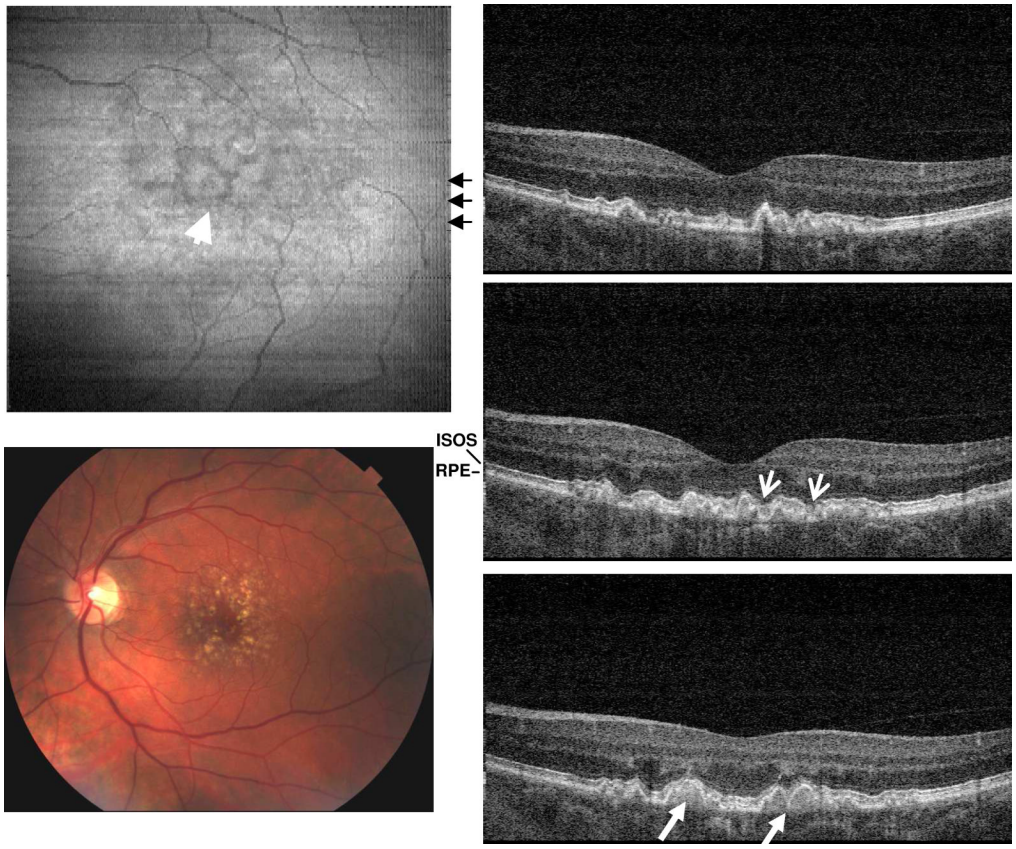


**Fig. 3.**

Image data from the left eye of a 60 year old female subject with dry AMD diagnosed in both eyes (View 3). Both *en face* OCT fundus image (left) and cross-sectional OCT (right) images show that the soft drusen have started to coalesce and form larger, confluent drusen. Three selected OCT cross-sectional images (right) clearly show the confluent drusen. Bruch's membrane cannot be identified as distinct from the drusen. The en face OCT fundus image also shows the smooth border between confluent drusen.

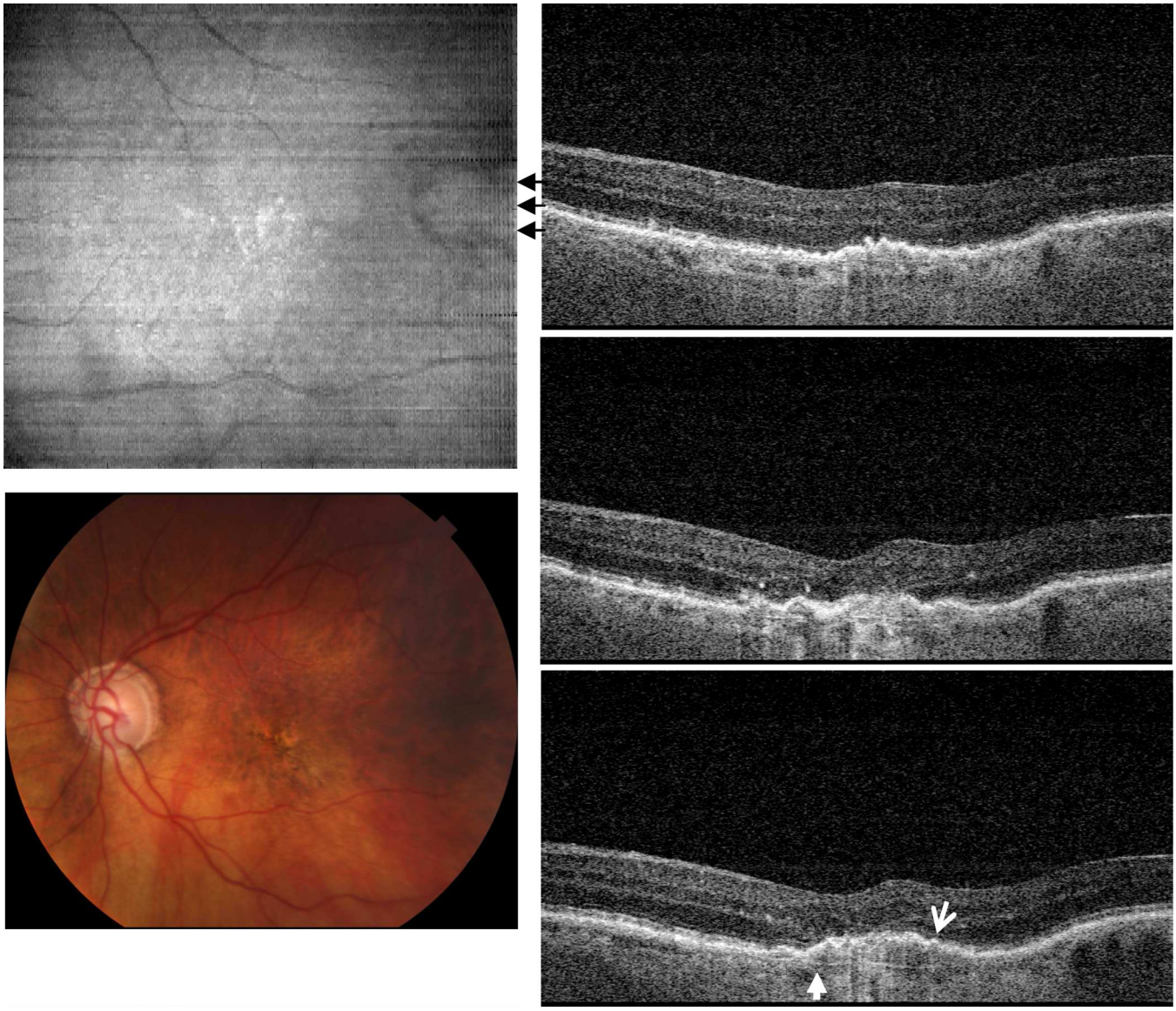

**Fig. 4.**

Image data from the left eye of a 91 year old female subject with AMD (View 4). A large retinal pigment epithelial detachment (PED) can be seen in the macula. The subject had a visual acuity of counting fingers at 5 feet (CF5'). The cross-sectional OCT images show many irregular scattering features and loss of photoreceptor integrity as evidenced by disruption of the photoreceptor inner and outer segment (IS/OS) boundary. Bruch's membrane is visible under the PED (solid arrow), but would not be visible in a normal retina. The inner retina is distorted by the elevation of the RPE and photoreceptors. Atrophy of the outer nuclear layer is also evident.

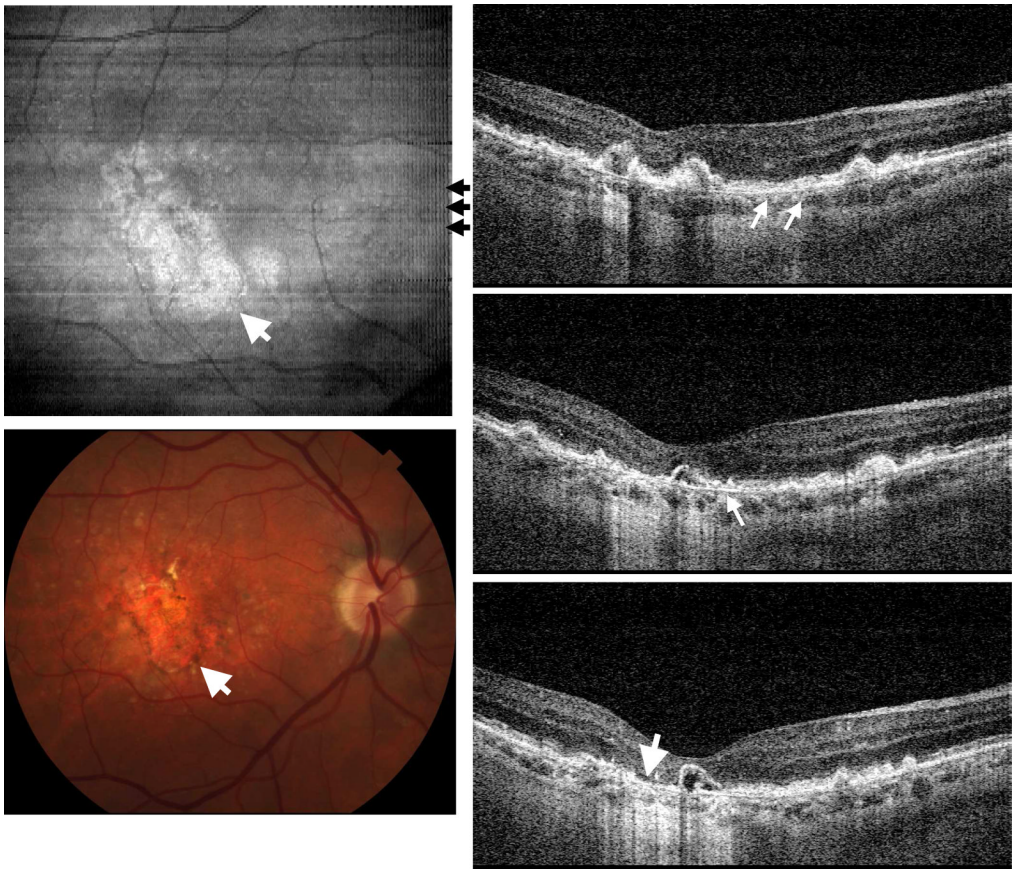

**Fig. 5.**

Image data from the right eye of a 67 year old male with dry AMD (View 5). Drusen deposit creates identifiable RPE and photoreceptor irregularities. The hyperscattering signal from the choroid beneath the lesion implies RPE atrophy. The IS/OS junction and RPE were no longer separable for UHR-OCT frames from the lesion area. Instead, the Bruch's membrane appeared under the RPE with a smooth contour.

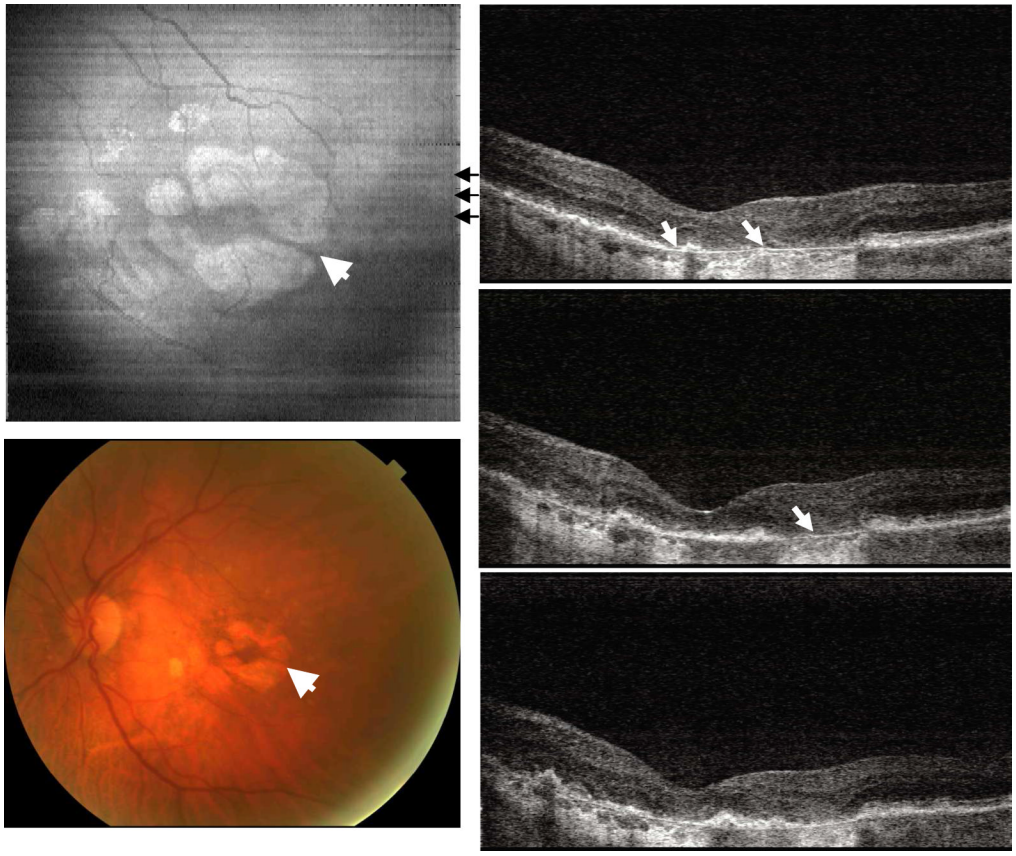

**Fig. 6.**

Image data from the left eye of an 84 year old female subject diagnosed with geographic atrophy and a visual acuity of 20/160 (View 6). Hyper-scattering appears on OCT images beneath the disrupted photoreceptor /RPE layers where Bruch's membrane can be easily identified. Both color photo and en face image of OCT demonstrate similar highly scattering area of RPE atrophy.

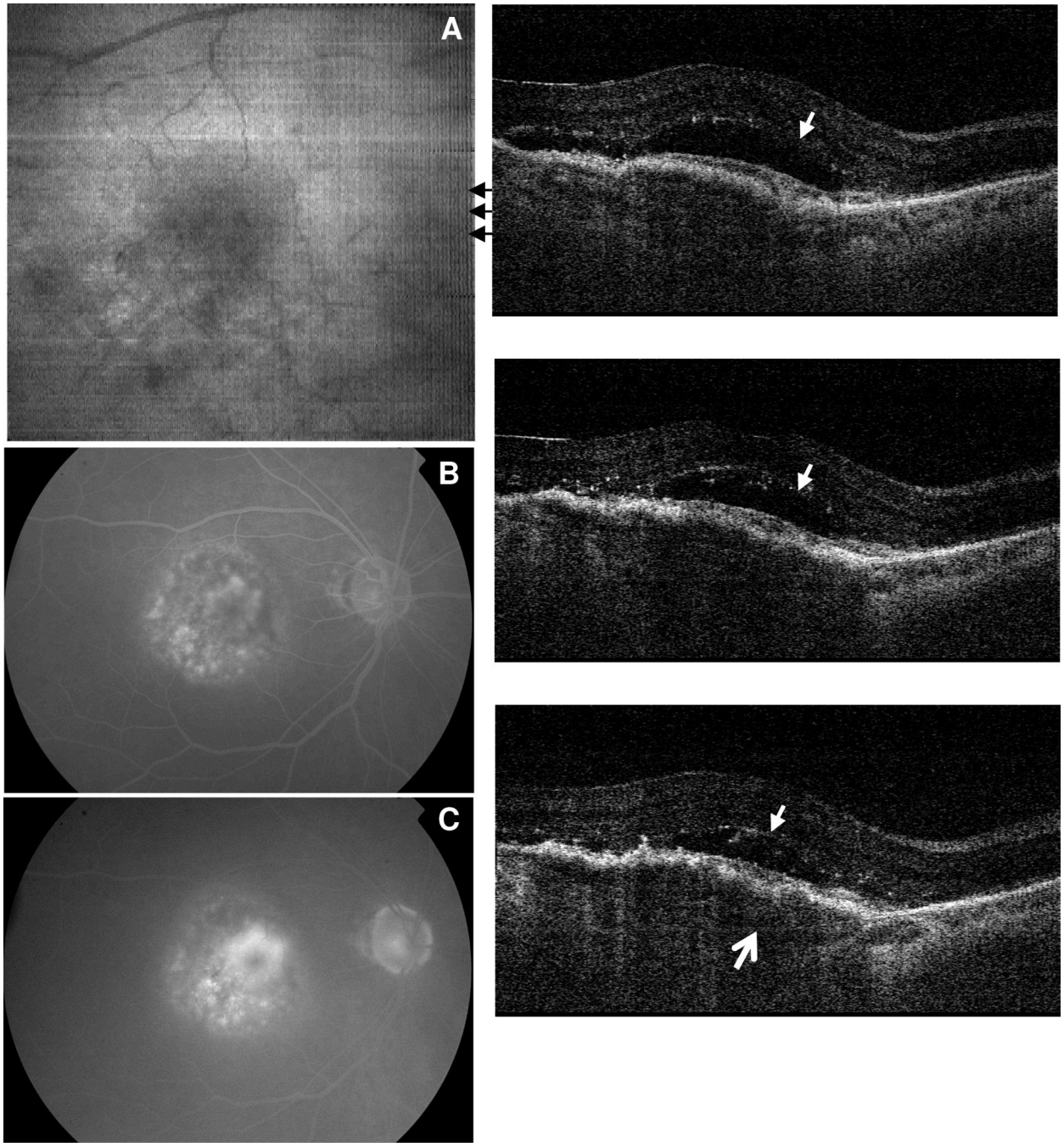


**Fig. 7.**

Image data from the right eye of a 77 year old female subject with wet AMD (View 7). Visual acuity was counting fingers at four feet. Fluorescein angiograms at 67 seconds (B) and 5 minutes and 8 seconds (C) indicate the development of choroidal neovascularization. A large volume of intraretinal fluid (small arrows) was identified from the OCT frames. The fluid developed over a large PED where the bottom arrow points the detached Bruch's membrane.

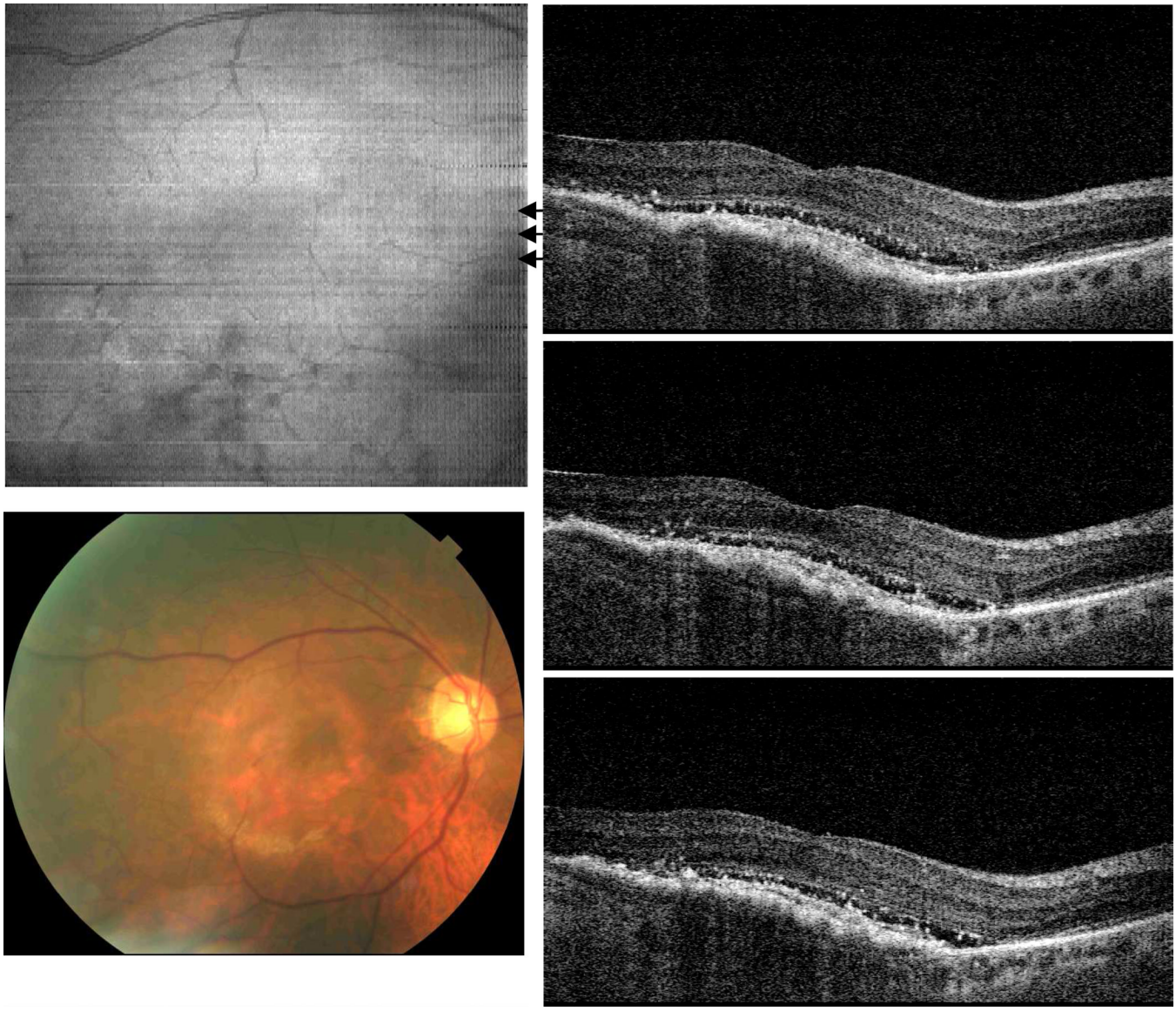

**Fig. 8.**

Image data from the same 77 year old female subject as in Fig. 7, after treatment with intravitreal ranibizumab (View 8). Visual acuity was counting fingers at five feet. OCT images show clearly reduced fluid volumes. Fluorescein angiography was not performed at this examination. The en face OCT fundus view exhibits a more uniform scattering intensity compared to that before treatment (Fig. 7).